(Received 12 January 2024, Accepted 4 March 2024, Scheduled 14 March 2024)

Exact Expressions for the Near Field of a Thin Uniform Circular Loop Current with Application to Loops Lying on a Half Space

David G. Miljak*

Commonwealth Scientific and Industrial Research Organisation, Lucas Heights, Australia

ABSTRACT: Exact analytic solutions for the electromagnetic field due to a thin, time varying uniform circular loop current are presented. The solutions are provided in the form of a power series with respect to wavenumber. The coefficients of the series are real functions of the spatial coordinates and loop radius and involve recursions of complete elliptic integrals or finite sums of elementary functions. Explicit expressions for the magnetic vector potential and electric and magnetic fields are provided for both cylindrical and spherical coordinate systems. The expressions are adapted for computing the electric field and axial magnetic field on the interface of two half spaces generated by a current loop lying on the half-space interface. Expressions for the self and mutual loop impedances are provided for both the free-space and interface case. Computed examples are given for specific frequency and half-space parameters and are compared to known solutions based on spherical Hankel functions or direct integration. The solutions are shown to be particularly efficient in the near field. Their derivation is motivated by recent developments of large sensors used in magnetic resonance sensing of minerals.

1. INTRODUCTION

There exists a very large body of literature relating to circular loop currents in free space, spanning a wide range of applications and results. Many studies have investigated loops as communication antennas for transmission and reception of propagating waves, providing expressions relating to loop impedance, radiation and associated fields [1–9]. Other work describes low frequency solutions for the current, impedance and fields of a thin loop or torus [10–13], formulation of generalised loop current distributions [14–16], mutual coupling of coaxial loops and their integration into coaxial arrays [17–19] as well as extensions to infinite conducting media [20, 21]. The collective work provides a rich understanding of loop radiation characteristics, coupling and field patterns, under a wide range of frequency, loop size, and method of excitation. Most studies provide results under certain simplifying assumptions, for example quasi-static approaches that ignore wave retardation effects, approximations of otherwise exact integral representations or idealised physical models involving infinitesimally thin current loops.

One specific longstanding research area involves the development of exact analytic solutions for the electromagnetic field due to an infinitesimally thin time varying loop current. Werner [6] provided exact series expressions for fields due to general loop current distributions based on a series of spherical Hankel functions, applicable to both near and far-field regions. Li et al. [7] provided an alternative representation involving spherical Hankel and Bessel functions, applicable to two distinct regions with spherical radii $r < a$ and $r > a$, where r is the radius of a sphere whose centre coincides with that of the loop and a is the loop radius. Expressions involving spherical Hankel functions have also been provided for the related problem of mutual coupling between coaxial loops sitting in parallel planes [17, 19]. These approaches provide significant computational speed advantages compared to numerical evaluation of integral representations. However, while these series solutions generally converge rapidly for positions far from the loop, in the near-field region the spherical functions are less well matched to the field distribution and consequently these series converge more slowly for field positions close to the loop.

Instead of expansion based on spherical waves, other functions may be used. For example, Maxwell provided a simple closed form expression for the field generated by a static loop current using complete elliptic integrals [10]. Overfelt [8] described a recurrence based on elliptic integrals for the case of a time varying uniform loop current, that is, where the current is constant along the loop contour, although the spatial region of validity was apparently restricted only to spherical radii $r > a$. Conway [9] provided a representation for general current distributions employing several nested sums of a recurrence of Legendre functions of the second kind, with validity over all space but with specific application to the near field. Both these later authors emphasised the much improved convergence properties of the respective series for positions close to the loop, compared to spherical waves.

In this paper, field representation based on a compact series involving complete elliptic integrals and elementary functions is developed for the case of uniform loop current and zero net charge, valid over all space for an infinite medium having simple dispersion. Explicit solutions are provided for the magnetic vector potential and electric and magnetic fields. The series are numerically compared to spherical wave solutions provided in [6]. Using the elliptic series, rapid convergence properties close to the loop in the near-field is demonstrated.

* Corresponding author: David G. Miljak (david.miljak@csiro.au).

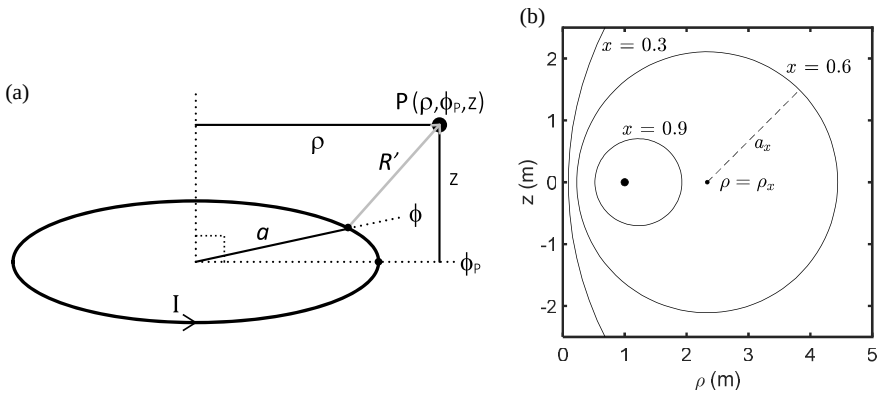

FIGURE 1. (a) Loop geometry and coordinate system, (b) selected toroidal surface cross sections corresponding to values of constant x for the case $a = 1$ m, as defined in Equation (5).

In addition, an exact series representation is derived for fields at the interface of two half spaces generated by a thin uniform loop current sitting on the half space interface. This specific loop configuration has been the subject of many investigations due to its importance for geoprospecting or surface wave propagation [22–29], metal detection [30, 31] and non-destructive analysis of materials [32]. Most approaches assume a uniform loop current but may either ignore displacement current, require a simplification of integral expressions or application of numerical methods. Recently however, exact expressions for a thin uniform loop current on a non-magnetic half space employing spherical functions have been published [27, 28]. On the other hand, the exact solution of this configuration presented in this paper is based on elliptic integrals. This solution is achieved by firstly considering known integral expressions for the fields in the interface and then exploiting the fact that the developed series expression for the infinite medium is a simple power series in wavenumber. The expressions allow the rapid computation of the self-impedance of a loop on a half space, as well as the mutual impedance of closely spaced loops that may form part of a larger coaxial array. Computational results are compared to the expressions employing spherical functions [27, 28].

The interest in efficient near-field representation is particularly motivated by the recent development of large magnetic resonance loop sensor arrays that are used for measurement of specific "zero-field" mineral resonances that occur in the HF to VHF range [33], operated both in air and over earth layers [34]. The sensing zone is generally limited to the extreme near field, corresponding to approximately one loop diameter from the loop centre. Coaxial loop arrays up to 5 m diameter have been operated at 18.5 MHz. This combination of loop size and frequency corresponds to strong phase shift in the near field where wave retardation effects are significant and where a simple quasi-static approach is no longer useful. Series expressions suited to near field calculation are especially useful for efficiently computing mutual and self impedances of closely spaced coaxial loop arrays to predict system radiation resistance and facilitate loop impedance matching. Computational efficiency is a particular advantage when optimising over a very large number of array configurations.

It should be noted that this and other analyses restricted to the assumption of uniform current have practical limitations with respect to loop modelling. The self-consistent spatial distribution of current and charge on a loop depends on the excitation method, for example, via an incident plane wave [14] or a voltage terminal [15, 16] and generally tends to nonuniformity when the loop circumference approaches a significant fraction of a wavelength in the medium. In such cases, a substantially uniform loop current may be imposed by employing phase shifters. For example, one strategy involves periodically loading capacitors along the loop circumference [35]. A substantially uniform current may be generated using this method, although a spatially periodic charge distribution is also developed along the loop which can generate fields and currents in the medium that cannot be modelled under a simple uniform current assumption. However, periodic charge distributions may be unimportant to the overall analysis if their characteristic dimensions remain sufficiently small compared to the medium wavelength such that they couple only weakly to radiation or, in the case of lossy media, localised power dissipation. To this extent, uniform loop current solutions remain of interest for analysing larger loops operated at higher frequency, as well as their coupling to coaxial elements.

2. MAGNETIC VECTOR POTENTIAL AND ELECTRIC FIELD

Figure 1(a) shows the cylindrical coordinate system, where an infinitesimally thin loop is immersed in an infinite medium and carries a current I uniformly distributed in the azimuthal direction. The loop sits in the plane $z = 0$ with the centre of the loop coincident with the coordinate system origin. Due to the uniform current assumption and circular symmetry the magnetic vector potential is independent of the azimuthal angle and only the azimuthal component A_ϕ of the potential is non-zero. The expression for A_ϕ at the field point $P(\rho, \phi_P, z)$ is given in [6] as

$$A_\phi = \frac{\mu_s I a}{2\pi} \int_0^\pi \frac{e^{-jk_s R'}}{R'} \cos\phi' d\phi', \tag{1a}$$

$$R' = \sqrt{a^2 + \rho^2 + z^2 - 2a\rho\cos\phi'},$$

$$k_s^2 \;=\; \omega^2\mu_s\epsilon_s - j\omega\mu_s\sigma_s, \tag{1b}$$

where k_s is the angular wavenumber (generally complex), ω the angular frequency, μ_s the medium permeability, ϵ_s the permittivity, and σ_s the conductivity. The integration variable is $\phi' = \phi - \phi_P$. The time variation $e^{j\omega t}$ is suppressed from the notation throughout.

The integral in (1a) may be split into two separate terms I_C and I_S by expanding the exponential factor using Euler's formula:

$$A_\phi \;=\; \frac{\mu_s I a}{2\pi}\,(I_C - jI_S)\,, \tag{2}$$

$$I_C \;=\; \int_0^\pi \frac{\cos k_s R'}{R'}\cos\phi' d\phi', \tag{3}$$

$$I_S \;=\; \int_0^\pi \frac{\sin k_s R'}{R'}\cos\phi' d\phi'. \tag{4}$$

I_C and I_S may be transformed by first making the following substitutions,

$$t = \cos\frac{\phi'}{2},\;\; \cos\phi' = 2t^2-1,\;\; R_o^2 = (a+\rho)^2 + z^2,$$
$$x^2 = \frac{4a\rho}{R_o^2}, \tag{5}$$

$$\cos k_s R' = \sum_{n=0}^{\infty}\frac{(-)^n}{(2n)!}\,(k_s R_o)^{2n}\,(1-x^2t^2)^n, \tag{6}$$

$$\frac{\sin k_s R'}{R'} = \sum_{m=0}^{\infty}\frac{(-)^m}{(2m+1)!}\,k_s\,(k_s R_o)^{2m}\big(1-x^2t^2\big)^m, \tag{7}$$

where the identities in (6) and (7), valid for complex k_s, follow from the Taylor expansion of $\cos k_s R'$ and $\sin k_s R'$ respectively and the use of the parameterisations in (5). The real dimensionless parameter x spans the range $0 \le x \le 1$. A constant value of x defines a toroidal surface nested around the current loop as shown in Figure 1(b); the toroidal surface major radius ρ_x and minor radius a_x are given by

$$\rho_x = a\varpi, \quad a_x = \frac{2a}{x^2}\sqrt{1-x^2}, \quad \varpi = \frac{2-x^2}{x^2}.$$

Values near $x = 1$ correspond to toroidal surfaces close to the loop contour while values near $x = 0$ correspond to surfaces that extend to regions distant from the loop. Substitution of (6) and (7) into (3) and (4) respectively yields

$$I_C \;=\; \frac{2}{R_o}\sum_{n=0}^{\infty}\frac{(-)^n}{(2n)!}\,(k_s R_o)^{2n}\,T_n\,(x)\,, \tag{8}$$

$$I_S \;=\; \frac{2}{R_o}\sum_{n=0}^{\infty}\frac{(-)^n}{(2n+3)!}\,(k_s R_o)^{2n+3}\,U_n(x), \tag{9}$$

$$\begin{aligned} T_n\,(x) \;&=\; \nu_n\,(x) - \varepsilon_n\,(x)\,,\\ U_n\,(x) \;&=\; h_n\,(x) - g_n(x), \end{aligned} \tag{10}$$

$$\begin{aligned} \nu_n(x) \;&=\; \int_0^1 \frac{2t^2(1-x^2t^2)^n}{\sqrt{1-x^2t^2}\sqrt{1-t^2}}\,dt,\\ \varepsilon_n(x) \;&=\; \int_0^1 \frac{(1-x^2t^2)^n}{\sqrt{1-x^2t^2}\sqrt{1-t^2}}\,dt, \end{aligned} \tag{11}$$

$$\begin{aligned} h_n\,(x) \;&=\; -\int_0^1 \frac{2t^2(1-x^2t^2)^{n+1}}{\sqrt{1-t^2}}\,dt,\\ g_n\,(x) \;&=\; -\int_0^1 \frac{(1-x^2t^2)^{n+1}}{\sqrt{1-t^2}}\,dt. \end{aligned} \tag{12}$$

where the indexing in (9) has been adjusted to omit the $m = 0$ term in (7), which integrates to zero after substituting into (4). Noting that

$$\nu_n = \frac{2}{x^2}\,(\varepsilon_n - \varepsilon_{n+1})\,,\quad h_n = \frac{2}{x^2}\,(g_n - g_{n+1})\,,\quad x \neq 0,$$

and substitution into the respective relations in (10) results in

$$T_n\,(x) \;=\; \varpi\varepsilon_n - \frac{2}{x^2}\,\varepsilon_{n+1}, \tag{13}$$

$$U_n\,(x) \;=\; \varpi g_n - \frac{2}{x^2}\,g_{n+1}. \tag{14}$$

Expressions for ε_n are given in [36] (p199, adapted from 331.00) as follows:

$$\varepsilon_0 \;=\; K\,(x)\,,\;\; \varepsilon_1 = E\,(x)\,, \tag{15}$$

$$\begin{aligned} \varepsilon_n \;&=\; \left(\frac{2n-2}{2n-1}\right)\kappa_2\varepsilon_{n-1} - \left(\frac{2n-3}{2n-1}\right)\kappa_1\varepsilon_{n-2},\\ &\qquad n>1,\;\; \kappa_1 = 1-x^2,\;\; \kappa_2 = 2-x^2. \end{aligned} \tag{16}$$

where $K(x)$ and $E(x)$ are the complete elliptic integrals of the first and second kind respectively and where x serves as the elliptic modulus. Other recursions for T_n may be obtained through rearrangements of (13) and (16), including:

$$T_n \;=\; -\frac{1}{x^2}\left(\frac{2n-1}{2n+1}\right)\{\kappa_2\varepsilon_n - 2\kappa_1\varepsilon_{n-1}\}\,, \tag{17a}$$

$$T_n \;=\; +\frac{1}{\kappa_2}\left(\frac{2n-1}{2n+1}\right)\{2\kappa_1 T_{n-1} - x^2\varepsilon_n\}\,, \tag{17b}$$

$$T_n \;=\; +\frac{1}{2}\left(\frac{2n-1}{2n+1}\right)\{\kappa_2 T_{n-1} - x^2\varepsilon_{n-1}\}\,, \tag{17c}$$

$$T_n \;=\; +\left(\frac{2n-1}{2n+1}\right)\{T_{n-1} + \varepsilon_n - \varepsilon_{n-1}\}\,. \tag{17d}$$

For the range $0 < x < 1$, $\varepsilon_n(x) > 0$ for all n and slowly decreases monotonically with increasing n, while $T_0(x) > 0$ and $T_n(x) < 0$ for $n > 0$ and also varies slowly as n increases.

To compute T_n, T_0 is first obtained by substituting the value of ε_0 and ε_1 defined in (15) into (13):

$$T_0\,(x) = \varpi K\,(x) - \frac{2}{x^2}\,E(x). \tag{18}$$

Then, for $n > 0$, T_n may be determined using any of (13) or (17), along with the use of (16) to compute one upgrade of either ε_{n-1}, ε_n or ε_{n+1}, depending on choice of recursion. For recursions (17b)–(17d), T_0 is directly used to seed the start of the recursion.

In contrast to the required recursion for calculating T_n, U_n may be obtained by direct evaluation of both g_n and h_n in (12), yielding the following elementary finite sum:

$$U_n(x) = \pi(n+1)! \sum_{k=1}^{n+1} (-)^{k+1} \left(\frac{x}{2}\right)^{2k} c_{nk},$$
$$c_{nk} = \frac{(2k-1)!}{(k+1)!\,(k-1)!(k-1)!\,(n-k+1)!}, \tag{19}$$

where use has been made of the identity in [37], Equation (3.248.3), p324,

$$\int_0^1 \frac{t^{2k}}{\sqrt{1-t^2}}\,dt = \frac{\pi}{2}\frac{(2k-1)!!}{(2k)!!}.$$

An alternative expression for $U_n(x)$ may be derived by starting with a different identity to (7):

$$\frac{\sin k_s R'}{R'} = \sum_{m=0}^{\infty} \frac{(-)^m}{(2m+1)!} k_s (k_s R_o)^{2m} \left(\frac{\varpi x^2}{2}\right)^m \left(1 - \frac{\cos\phi'}{\varpi}\right)^m. \tag{20}$$

Comparison of (20) with (4) and (7) allows one to infer that

$$U_n = \left(\frac{\varpi x^2}{2}\right)^{n+1} \int_0^{\pi} \left(1 - \frac{\cos\phi'}{\varpi}\right)^{n+1} \cos\phi' d\phi'.$$

Collecting all even powers of $\cos\phi'$ in the integrand and noting that odd powers integrate to zero, one obtains

$$U_n(x) = \pi(n+1)! \left(\frac{\kappa_2}{2}\right)^{n+1} \sum_{k=1}^{\frac{n}{2}+1} p_{nk} \varpi^{1-2k}, \tag{21}$$
$$p_{nk} = \frac{1}{2^{2k} k!\,(k-1)!\,(n-2k+2)!},$$

where use has been made of the following identity in [37], Equation (2.512.2),

$$\int_0^{\pi} \cos^{2k}\phi' d\phi' = \pi \frac{(2k-1)!!}{(2k)!!}.$$

Equation (21) directly demonstrates that $U_n(x) \geq 0$ for all n and x. Expressions for the first few U_n are given by

$$U_0 = \pi\left(\frac{x^2}{8}\right), \quad U_1 = \pi\left(\frac{x^2}{4} - \frac{x^4}{8}\right),$$
$$U_2 = \pi\left(\frac{3x^2}{8} - \frac{3x^4}{8} + \frac{15x^6}{128}\right).$$

Finally, combining Equations (2), (8), and (9), the series for A_ϕ may be written as

$$A_\phi(\rho,z) = \frac{\mu_s I a}{\pi R_o} \sum_{n=0}^{\infty} (-)^n (k_s R_o)^{2n} \left\{ \frac{T_n(x)}{(2n)!} - j\frac{(k_s R_o)^3 U_n(x)}{(2n+3)!} \right\}, \tag{22}$$

where $T_n(x)$ is given by (13) or (17), and $U_n(x)$ is given by (19) or (21). The expression for A_ϕ in (22) is a power series in the complex wavenumber k_s. The real coefficients T_n and U_n depend only on the loop radius and field coordinate (ρ, z). When $k_s = 0$ (low frequency limit) the only contribution to the sum in (22) is provided by the $n = 0$ term so that

$$A_\phi|_{k_s=0} = \frac{\mu_s I a}{\pi R_o} T_0(x),$$

which is the result for A_ϕ due to a static current. Under the assumption of uniform current and zero net loop charge the total electric field is given by

$$E_\phi(\rho,z) = -j\omega A_\phi = -\frac{\mu_s \omega I a}{\pi R_o} \sum_{n=0}^{\infty} (-)^n (k_s R_o)^{2n} \left\{ \frac{(k_s R_o)^3 U_n(x)}{(2n+3)!} + j\frac{T_n(x)}{(2n)!} \right\}. \tag{23}$$

The mutual impedance between two coaxial loops of radius a and $\rho = b$, sitting in parallel planes separated by z is therefore given by

$$Z_{ab} = \frac{-2\pi b E_\phi}{I} = \frac{2\mu_s \omega a b}{R_o} \sum_{n=0}^{\infty} (-)^n (k_s R_o)^{2n} \left\{ \frac{(k_s R_o)^3 U_n(x)}{(2n+3)!} + j\frac{T_n(x)}{(2n)!} \right\}. \tag{24}$$

When k_s is real, such as for the free-space wavenumber k_0, the expression for Z_{ab} has a real part (mutual resistance) contributed entirely by the U_n terms, while the imaginary part (mutual reactance) has contributions only from the T_n terms. Mixed contributions occur for complex k_s.

It is interesting to consider the case $x = 1$, which corresponds to $b = a$, i.e., field points coincident with the loop itself, where the loop mutual impedance collapses to the self impedance. The U_n coefficients are valid over all space, including the loop contour. The T_n have validity for $0 < x \leq 1$ except for T_0, which diverges logarithmically at $x = 1$ since $K(x) \to \ln(4/\sqrt{1-x^2})$ as $x \to 1$ in the expression for T_0 in (18). The divergence of this single term, which only occurs when considering the loop self reactance, is associated with the known divergence of the quasi-static impedance due to the assumed idealised infinitesimal loop thickness. A resolution of

the divergence of T_0 may be obtained by assuming a non-zero but small loop wire radius δ, so that

$$T_0(1) \to T_\delta, \quad T_\delta \approx \ln\left(\frac{8a}{\delta}\right) - 2,$$

where T_δ yields the known quasistatic reactance of a thin torus assumed to have a toroidal surface current evenly distributed around the torus poloidal direction [11, p111]. Besides this modification, the infinitesimal loop assumption is maintained for $n > 0$ terms, where the T_n remain finite at $x = 1$, since $(x^2-1)\varepsilon_n \to 0$ as $x \to 1$ for any ε_n in (16). Consequently (13) may be safely used to generate the T_n terms starting at T_1, using $\varepsilon_2 = 2\varepsilon_1/3$. Under these assumptions, the loop self impedance is given as:

$$Z_{aa} = \mu_s \omega a \left[jT_\delta + \sum_{n=0}^{\infty} (-)^n (k_s a)^{2n+2} \{k_s a S_n + jC_n\} \right], \tag{25}$$

$$C_n = \frac{2^{2n+1}(2n+1)}{(n+1)(2n+1)!!(2n+3)!!}, \tag{26}$$

$$S_n = \frac{\pi}{(n)!(n+2)!(2n+3)}, \tag{27}$$

where C_n and S_n result from considerable simplification for $T_{n+1}(1)$ and $U_n(1)$ respectively and where the quasistatic term T_δ is explicitly drawn out of the sum as the substitution for $T_0(1)$. Equation (25) essentially corresponds to a simplified version of the series involving gamma functions provided in [5], Equation (14), applied to the particular case of uniform current. Equation (27) has also been derived in a different manner in [4].

3. MAGNETIC FIELD EXPRESSIONS

The magnetic fields may be obtained by evaluating $B = \nabla \times A$ in cylindrical coordinates:

$$B_\rho = -\frac{\partial}{\partial z} A_\phi, \tag{28}$$

$$B_z = \frac{1}{\rho}\frac{\partial}{\partial \rho}(\rho A_\phi). \tag{29}$$

Substituting (22) into (28) and noting that $\frac{\partial}{\partial z}(R_o^2 U_0) = 0$ gives the following for B_ρ:

$$B_\rho(\rho, z) = -\frac{\mu_s I a z}{\pi R_o^3} \sum_{n=0}^{\infty} (-)^n (k_s R_o)^{2n} \left\{ \frac{D_n^{(\rho)}}{(2n)!} + j \frac{(k_s R_o)^5 G_n^{(\rho)}}{(2n+5)!} \right\}, \tag{30}$$

where $D_n^{(\rho)}$ is given by the following recursion, where in what follows $K(x)$ and $E(x)$ are simply denoted as K and E respectively:

$$D_0^{(\rho)} = \frac{1}{x^2}\left(2K - \frac{E\kappa_2}{\kappa_1}\right), \tag{31}$$

$$D_n^{(\rho)} = \left(\frac{2n-1}{2n+1}\right)\left\{D_{n-1}^{(\rho)} + \xi_n^{(\rho)} - \xi_{n-1}^{(\rho)} - 4\varepsilon_{n-1}\right\} \quad n > 0, \tag{32}$$

$$\xi_0^{(\rho)} = -\left(\frac{4K}{x^2} + \frac{E}{\kappa_1}\right), \quad \xi_1^{(\rho)} = K - \frac{4E}{x^2}, \tag{33}$$

$$\xi_n^{(\rho)} = \left(\frac{2n-2}{2n-1}\right)\left\{\kappa_2 \xi_{n-1}^{(\rho)} + 4\varepsilon_{n-1}\right\} - \left(\frac{2n-3}{2n-1}\right)\left\{\kappa_1 \xi_{n-2}^{(\rho)} + 2\kappa_2 \varepsilon_{n-2}\right\} \quad n > 1, \tag{34}$$

and where $G_n^{(\rho)}$ is given by

$$G_n^{(\rho)} = (2n+4) U_n. \tag{35}$$

The form of $D_n^{(\rho)}$ in (32) is derived from the specific recursion for T_n in (17d); related versions of $D_n^{(\rho)}$ may be developed based on the other recursions in (17). The practical computation of the $D_n^{(\rho)}$ proceeds in a similar manner to that for T_n previously described, except that both ε_{n-1} using (16) and then $\xi_n^{(\rho)}$ using (34) are updated to compute the nth recursion. The derivation of the these and subsequent results in this section are facilitated by using identities for elliptic integral derivatives with respect to modulus provided in [36], p282.

Using a similar procedure to the derivation of (30)–(35), substitution of (22) into (29) yields the following expression for B_z:

$$B_z(\rho, z) = \frac{\mu_s I a q}{\pi R_o^3} \sum_{n=0}^{\infty} (-)^n (k_s R_o)^{2n} \left\{ \frac{D_n^{(z)}}{(2n)!} - j \frac{(k_s R_o)^3 G_n^{(z)}}{(2n+3)!} \right\}, \tag{36}$$

where

$$q = a\varpi - \rho, \quad \psi = \frac{a+\rho}{q}, \quad \eta = \psi\varpi - 1,$$

$$D_0^{(z)} = K\eta - E\left(\frac{\eta - \psi}{\kappa_1}\right), \tag{37}$$

$$D_n^{(z)} = \left(\frac{2n-1}{2n+1}\right)\left\{D_{n-1}^{(z)} + \xi_n^{(z)} - \xi_{n-1}^{(z)} - 4\psi\varepsilon_{n-1}\right\}, \quad n > 0 \tag{38}$$

$$\xi_0^{(z)} = \frac{E}{\kappa_1} - K\left(\eta + \frac{2\psi}{x^2}\right),$$

$$\xi_1^{(z)} = E(1 + \psi - 2\eta) - K, \tag{39}$$

$$\xi_n^{(z)} = \left(\frac{2n-2}{2n-1}\right)\left\{\kappa_2 \xi_{n-1}^{(z)} + 2x^2\eta\varepsilon_{n-1}\right\} - \left(\frac{2n-3}{2n-1}\right)\left\{\kappa_1 \xi_{n-2}^{(z)} + 2x^2(\eta - \psi)\varepsilon_{n-2}\right\} \quad n > 1, \tag{40}$$

and

$$G_n^{(z)} = 2\pi\,(n+1)!\left(\frac{\kappa_2}{2}\right)^n \sum_{k=1}^{\frac{n}{2}+1} p_{nk}\varpi^{1-2k} \left\{2k+\frac{\rho}{q}(n+2)\right\}, \quad (41)$$

where the specific form of $G_n^{(z)}$ in (41) is derived from (21); equivalent elementary sums for $G_n^{(z)}$ may also be derived from (19).

The expressions (30) and (36) for B_ρ and B_z are valid for all space except for $x = 0$ (loop axis) and $x = 1$ (loop contour). For the case of $\rho = x = 0$, $B_\rho = 0$ while B_z on the loop axis can be evaluated by noting the following limits:

$$\lim_{x\to 0}\left(\xi_n^{(z)} - \xi_{n-1}^{(z)}\right) = 0, \quad \lim_{x\to 0}\varepsilon_{n-1} = \frac{\pi}{2}, \quad n > 0$$

$$\lim_{x\to 0}\left(qx^2\right) = 2a, \quad \lim_{x\to 0}\left(qD_n^{(z)}\right) = \frac{2\pi a}{2n+1}\left(\frac{1}{4} - n^2\right),$$

and the additional known limit [36], p11

$$\lim_{x\to 0}\left(\frac{K-E}{x^2}\right) = \frac{\pi}{4}.$$

Applying these limits to (37)–(41) and substituting resulting terms into (36) gives

$$B_z\,(0,z) = B_{zo}\sum_{n=0}^{\infty}(-)^n\,(k_sR_o)^{2n}\left\{\frac{(1-2n)}{(2n)!} - j\,\frac{(k_sR_o)^3\,(2n+2)}{(2n+3)!}\right\}, \quad (42)$$

$$B_{zo} = \frac{\mu_s I a^2}{2R_o^3}.$$

When $k_s = 0$, $B_z(0,z)$ reduces to B_{zo} which is the known relation for the on-axis field due to a static current. Equation (42) is also identified as the series equivalent to $B_z(0,z)$ derived from the spherical Hankel expansion adapted from [6], Equation (57):

$$B_z\,(0,z) = B_{zo}\left\{(\cos k_sR_o + k_sR_o\sin k_sR_o) - j\,(\sin k_sR_o - k_sR_o\cos k_sR_o)\right\}. \quad (43)$$

For completeness, direct expressions for the magnetic field components in spherical coordinates (r,θ,ϕ) are obtained by evaluating the following expressions:

$$B_r = \frac{1}{r\sin\theta}\frac{\partial}{\partial\theta}\left(\sin\theta A_\phi\right), \quad (44)$$

$$B_\theta = -\frac{1}{r}\frac{\partial}{\partial r}\left(rA_\phi\right). \quad (45)$$

where R_o^2 and x^2 are expressed in spherical coordinates as follows:

$$R_o^2 = a^2 + r^2 + 2ar\sin\theta, \quad x^2 = \frac{4ar\sin\theta}{R_o^2}.$$

The resulting series for B_r is

$$B_r\,(r,\theta) = \frac{\mu_s I a}{\pi R_o}\left(\frac{\cot\theta}{4r}\right)\sum_{n=0}^{\infty}(-)^n\,(k_sR_o)^{2n}\left\{\frac{D_n^{(r)}}{(2n)!} - j\,\frac{(k_sR_o)^3\,G_n^{(r)}}{(2n+3)!}\right\}, \quad (46)$$

where

$$D_0^{(r)} = E\,\frac{x^2}{\kappa_1}, \quad (47)$$

$$D_n^{(r)} = \left(\frac{2n-1}{2n+1}\right)\left\{D_{n-1}^{(r)} + \xi_n^{(r)} - \xi_{n-1}^{(r)} - 4x^2\varepsilon_{n-1}\right\}, \quad n > 0 \quad (48)$$

$$\xi_0^{(r)} = E\,\frac{\kappa_2}{\kappa_1} - 2K, \quad \xi_1^{(r)} = 2E - \kappa_2 K, \quad (49)$$

$$\xi_n^{(r)} = \left(\frac{2n-2}{2n-1}\right)\left\{\kappa_2\xi_{n-1}^{(r)}\right\} - \left(\frac{2n-3}{2n-1}\right)\left\{\kappa_1\xi_{n-2}^{(r)} - 2x^4\varepsilon_{n-2}\right\}, \quad n > 1 \quad (50)$$

and where

$$G_n^{(r)} = 2\pi\,(n+1)!\left(\frac{\kappa_2}{2}\right)^{n+1}\sum_{k=1}^{\frac{n}{2}+1} p_{nk}\varpi^{1-2k}\left\{4k\right\}. \quad (51)$$

Similarly, the series for B_θ is

$$B_\theta\,(r,\theta) = -\frac{\mu_s I a}{\pi r R_o}\sum_{n=0}^{\infty}(-)^n\,(k_sR_o)^{2n}\left\{\frac{D_n^{(\theta)}}{(2n)!} - j\,\frac{(k_sR_o)^3\,G_n^{(\theta)}}{(2n+3)!}\right\}, \quad (52)$$

where

$$\vartheta = 4 - x^2 - \frac{4a^2}{R_o^2},$$

$$D_0^{(\theta)} = \frac{1}{2x^2}\left\{K\left(\vartheta - x^2\right) - E\left(\frac{\kappa_2\vartheta - 2x^2}{2\kappa_1}\right)\right\}, \quad (53)$$

$$D_n^{(\theta)} = \left(\frac{2n-1}{2n+1}\right)\left\{D_{n-1}^{(\theta)} + \xi_n^{(\theta)} - \xi_{n-1}^{(\theta)} - \vartheta\varepsilon_{n-1}\right\}, \quad n > 0 \quad (54)$$

$$\xi_0^{(\theta)} = K\left(\frac{1}{2} - \frac{\vartheta}{x^2}\right) - E\left(\frac{\vartheta - 2}{4\kappa_1}\right),$$

$$\xi_1^{(\theta)} = K\left(\frac{\vartheta-2}{4}\right)+E\left(\frac{3}{2}-\frac{\vartheta}{x^2}\right), \quad (55)$$

$$\xi_n^{(\theta)} = \left(\frac{2n-2}{2n-1}\right)\left\{\kappa_2\xi_{n-1}^{(\theta)}+(\vartheta-x^2)\varepsilon_{n-1}\right\}-\left(\frac{2n-3}{2n-1}\right) \left\{\kappa_1\xi_{n-2}^{(\theta)}+\left(\frac{\kappa_2\vartheta}{2}-x^2\right)\varepsilon_{n-2}\right\} \quad n>1, \quad (56)$$

and where

$$G_n^{(\theta)} = \pi(n+1)!\left(\frac{\kappa_2}{2}\right)^n\sum_{k=1}^{\frac{n}{2}+1}p_{nk}\varpi^{1-2k} \left\{\left(\vartheta-x^2\right)\left(\frac{n}{2}+1\right)-k\left(\vartheta-2\right)\right\}. \quad (57)$$

4. APPLICATION TO LOOPS LYING ON A HALF-SPACE

The total electric field E_T generated by a uniform loop current above the surface of a semi-infinite half space is given by the following Sommerfeld-type integrals [32]:

$$E_T(\rho,z) = -\frac{j\mu_0\omega Ia}{2}(P+Q), \quad (58)$$

$$P = \int_0^\infty \frac{e^{-u_o|z-h|}}{u_o}k_\rho J_1(k_\rho a)J_1(k_\rho\rho)\,dk_\rho, \quad (59)$$

$$Q = \int_0^\infty R\frac{e^{-u_o(z+h)}}{u_o}k_\rho J_1(k_\rho a)J_1(k_\rho\rho)\,dk_\rho, \quad (60)$$

$$R = \frac{u_0-u_1}{u_0+u_1}, \quad u_0=\sqrt{k_\rho^2-k_0^2}, \quad u_1=\sqrt{k_\rho^2-k_1^2},$$

where the half space surface is located at $z=0$; h is the height of the loop above the surface; k_0 and k_1 are the wavenumbers above and below the surface, respectively; and k_ρ is the radial wavenumber component. J_1 is the Bessel function of the first kind with unity order. R is the plane wave reflection coefficient limited to the case where the half space is non-magnetic, i.e., permeability equal to the free space permeability μ_0. E_T is confined to the azimuthal direction and is independent of ϕ. The integral P accounts for the electric field normally generated by the loop current in an infinite medium in the absence of the half space, while the integral Q represents the secondary field due to reflection of waves off the surface. The exponential terms in P and Q tend to unity as the planes of the loop and the field point approach the surface.

The reflection coefficient may also be written as:

$$R = \frac{(u_0-u_1)^2}{k_1^2-k_0^2} = \frac{2(u_0^2-u_0u_1)}{\gamma^2}-1, \quad (61)$$

$$\gamma^2 = k_1^2-k_0^2.$$

Substitution of the form of R in (61) into (60) with $h=0$ leads to the following limit for the electric field E_{T0} on the surface:

$$E_{T0}(\rho) = \lim_{z\to0}E_T = -\frac{j\mu_0\omega Ia}{\gamma^2}\int_0^\infty (u_o-u_1) k_\rho J_1(k_\rho a)J_1(k_\rho\rho)\,dk_\rho. \quad (62)$$

The objective is to find a series expansion for (62). To proceed, we consider the following differential operator L and the integral P (with $h=0$) cast as functions of a general wavenumber variable k_s:

$$L = k_s\left(1+z\frac{\partial}{\partial z}\right), \quad (63)$$

$$P(k_s) = \int_0^\infty \frac{e^{-u_sz}}{u_s}k_\rho J_1(k_\rho a)J_1(k_\rho\rho)\,dk_\rho,$$

$$u_s = \sqrt{k_\rho^2-k_s^2}.$$

Noting that

$$\frac{\partial P(k_s)}{\partial z} = -\int_0^\infty e^{-u_sz}k_\rho J_1(k_\rho a)J_1(k_\rho\rho)\,dk_\rho,$$

application of the operator L to $P(k_s)$ gives

$$L[P(k_s)] = \int_0^\infty k_se^{-u_sz}\left(\frac{1}{u_s}-z\right) k_\rho J_1(k_\rho a)J_1(k_\rho\rho)\,dk_\rho. \quad (64)$$

Assuming the form of the dispersion relation in (1b), then based on physical grounds $P(k_s)$ and its spatial derivatives are analytic functions of k_s and therefore $L[P(k_s)]$ may be integrated with respect to k_s between two complex values $k_s=k_0$ and $k_s=k_1$ along any path:

$$F(\rho,z) = \int_{k_0}^{k_1}L[P(k_s)]\,dk_s = \int_{k_0}^{k_1}\int_0^\infty k_se^{-u_sz} \left(\frac{1}{u_s}-z\right)k_\rho J_1(k_\rho a)J_1(k_\rho\rho)\,dk_\rho dk_s$$

Changing the order of integration gives

$$F(\rho,z) = \int_0^\infty\left(\int_{k_0}^{k_1}k_se^{-u_sz}\left(\frac{1}{u_s}-z\right)dk_s\right) k_\rho J_1(k_\rho a)J_1(k_\rho\rho)\,dk_\rho. \quad (65)$$

The bracketed integral may be evaluated by noting that

$$\frac{\partial}{\partial k_s}\left(u_se^{-u_sz}\right) = -k_se^{-u_sz}\left(\frac{1}{u_s}-z\right)$$

so that

$$F(\rho,z) = \int_0^\infty\left(u_0e^{-u_0z}-u_1e^{-u_1z}\right) k_\rho J_1(k_\rho a)J_1(k_\rho\rho)\,dk_\rho. \quad (66)$$

The limit $z\to0$ $F(\rho,z)$ gives

$$F(\rho,0) = \int_0^\infty (u_0-u_1)k_\rho J_1(k_\rho a)J_1(k_\rho\rho)\,dk_\rho, \quad (67)$$

which is immediately identified as the limiting integral in (62), so that

$$E_{T0}(\rho) = -\frac{j\mu_0\omega Ia}{\gamma^2} F(\rho, 0). \quad (68)$$

The next step is to note that P is proportional to the power series (23) established for E_ϕ in an infinite medium, now explicitly separated into factors involving wavenumber and coordinates:

$$P(k_s) = -\frac{2}{j\mu_0\omega Ia} E_\phi = \sum_{n=0}^{\infty} \left\{k_s^{2n+3} V_n + j k_s^{2n} W_n\right\}, \quad (69)$$

$$V_n = \frac{2(-)^n R_o^{2n+2} U_n}{j\pi (2n+3)!}, \quad W_n = \frac{2(-)^n R_o^{2n-1} T_n}{j\pi (2n)!}.$$

The operator L and subsequent integration can then be trivially applied to (69) term by term, so that

$$F(\rho, z) = \sum_{n=0}^{\infty} \left\{ \left(\frac{k_1^{2n+5} - k_0^{2n+5}}{2n+5}\right) \left(V_n + z\frac{\partial V_n}{\partial z}\right) + j \left(\frac{k_1^{2n+2} - k_0^{2n+2}}{2n+2}\right) \left(W_n + z\frac{\partial W_n}{\partial z}\right)\right\}. \quad (70)$$

Substituting (70) into (68) and noting that the derivatives of V_n and W_n are finite, the electric field in the limit $z \to 0$ is given by

$$E_{T0}(\rho) = -\frac{2\mu_0\omega Ia}{\pi R_o \gamma^2} \sum_{n=0}^{\infty} (-)^n R_o^{2n} \left\{ \frac{R_o^3 \left(k_1^{2n+5} - k_0^{2n+5}\right)}{(2n+3)!\,(2n+5)} U_n + j \frac{\left(k_1^{2n+2} - k_0^{2n+2}\right)}{(2n)!\,(2n+2)} T_n \right\}, \quad (71)$$

where, in the interface, $R_o = \rho + a$.

An alternative expression for $E_{T0}(\rho)$ may be obtained by considering the Sommerfeld representation for the radial magnetic field in infinite non-magnetic media that follows from applying (28) to (59):

$$B_{\rho 0} = \frac{\mu_0 Ia}{2} \int_0^\infty e^{-u_o z} k_\rho J_1(k_\rho a) J_1(k_\rho \rho)\, dk_\rho,$$

$$B_{\rho 1} = \frac{\mu_0 Ia}{2} \int_0^\infty e^{-u_1 z} k_\rho J_1(k_\rho a) J_1(k_\rho \rho)\, dk_\rho,$$

where $B_{\rho 0}$ and $B_{\rho 1}$ are the radial fields (for $z > 0$) at the same field point for respective media having wavenumbers k_0 and k_1. Then

$$\frac{\partial}{\partial z}(B_{\rho 1} - B_{\rho 0}) = \frac{\mu_0 Ia}{2} \int_0^\infty \left(u_o e^{-u_o z} - u_1 e^{-u_1 z}\right) k_\rho J_1(k_\rho a) J_1(k_\rho \rho)\, dk_\rho. \quad (72)$$

Comparison of (72) with (66) leads to

$$E_{T0}(\rho) = -2\frac{j\omega}{\gamma^2} \lim_{z\to 0} \frac{\partial}{\partial z}(B_{\rho 1} - B_{\rho 0}). \quad (73)$$

The limit in (73) may be trivially evaluated directly from (30) so that

$$E_{T0}(\rho) = -\frac{2\mu_0\omega Ia}{\pi R_o \gamma^2} \sum_{n=0}^{\infty} (-)^n R_o^{2n} \left\{ \frac{R_o^3 \left(k_1^{2n+5} - k_o^{2n+5}\right)}{(2n+5)!} G_n^{(\rho)} + j \frac{\left(k_1^{2n+2} - k_o^{2n+2}\right)}{(2n+2)!} D_{n+1}^{(\rho)} \right\}, \quad (74)$$

where $D_{n+1}^{(\rho)}$ and $G_n^{(\rho)}$ may be computed using (32) and (35) respectively.

By consideration of (24) and using the form of E_{T0} in (71), it follows that the mutual impedance Z_{ab0} between two coaxial loops on the surface with radii a and b, i.e., $R_o = a + b$, is

$$Z_{ab0} = \frac{4\mu_0\omega ab}{R_o\gamma^2} \sum_{n=0}^{\infty} (-)^n R_o^{2n} \left\{ \frac{R_o^3 \left(k_1^{2n+5} - k_0^{2n+5}\right)}{(2n+3)!\,(2n+5)} U_n + j \frac{\left(k_1^{2n+2} - k_0^{2n+2}\right)}{(2n)!\,(2n+2)} T_n \right\}. \quad (75)$$

The self-impedance Z_{aa0} of a loop on the interface follows from a similar procedure used to derive (25) and is given by

$$Z_{aa0} = \mu_0\omega a \left[jT_\delta + \frac{2}{\gamma^2} \sum_{n=0}^{\infty} (-)^n a^{2n+2} \left\{ \frac{a(k_1^{2n+5} - k_0^{2n+5})}{2n+5} S_n + j \frac{(k_1^{2n+4} - k_0^{2n+4})}{2n+4} C_n \right\} \right] \quad (76)$$

where C_n and S_n may be computed using (26) and (27) respectively.

The axial magnetic field on the interface, B_{T0z}, may be obtained by tracing a similar procedure for deriving the electric field given in (71). The Sommerfeld representation of the total axial field above the interface, stemming from application of (29) to (58), is given by

$$B_T = \frac{\mu_0 Ia}{2} \int_0^\infty \left(\frac{e^{-u_o|(z-h)|}}{u_o} + R \frac{e^{-u_o(z+h)}}{u_o} \right) k_\rho^2 J_1(k_\rho a) J_0(k_\rho \rho)\, dk_\rho, \quad (77)$$

so that

$$B_{T0z}(\rho) = \frac{2\mu_0 Iaq}{\pi\gamma^2 R_o^3} \sum_{n=0}^{\infty} (-)^n R_o^{2n} \left\{ \frac{(k_1^{2n+2} - k_0^{2n+2})}{(2n)!(2n+2)} D_n^{(z)} - j \frac{R_o^3 \left(k_1^{2n+5} - k_0^{2n+5}\right)}{(2n+3)!(2n+5)} G_n^{(z)} \right\}, \quad (78)$$

where $D_n^{(z)}$ and $G_n^{(z)}$ are defined in (38) and (41), respectively. The axial field at the centre of the loop is obtained by using the same simplification of $D_n^{(z)}$ and $G_n^{(z)}$ used in (42) for $\rho = 0$, now with $R_o = a$, leading to

$$B_{T0z}(0) = \frac{\mu_0 I}{a\gamma^2} \sum_{n=0}^{\infty} (-)^n a^{2n} \left\{ \frac{(1-2n)(k_1^{2n+2} - k_0^{2n+2})}{(2n)!(2n+2)} \right.$$

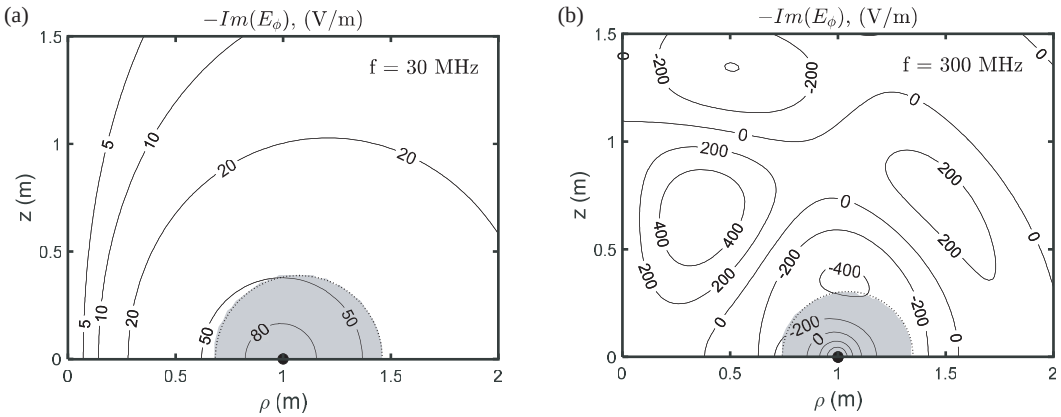

FIGURE 2. Contour plots of $-\mathrm{Im}(E_\phi)$ for a loop with $a = 1$ m and $I = 1$ A in the extreme near-field zone using Equations (17d) and (23). (a) 30 MHz and (b) 300 MHz. Shaded zones indicate loss of accuracy for computations using spherical solutions.

$$-j\,\frac{a^3\,(2n+2)\left(k_1^{2n+5}-k_0^{2n+5}\right)}{(2n+3)!(2n+5)}\Bigg\}. \qquad (79)$$

Equation (79) is identified as the equivalent power series for the closed form of $B_{T0z}(0)$ given in [27], Equation (51), simplified for the case of $\rho = 0$,

$$B_{T0z}\,(0) = -\frac{j\mu_0 I}{\gamma^2}\left\{k_1^3 h_2^{(2)}\,(k_1 a) - k_0^3 h_2^{(2)}\,(k_0 a)\right\},$$

where $h_2^{(2)}(\cdot)$ is the second order spherical Hankel function of the second kind.

For the case of the radial field in the interface, it appears that the method used above cannot be readily adapted to provide a solution. However, the radial field in the interface is provided in [27] as a recursion involving Bessel function products.

5. RESULTS FOR FREE SPACE

As described in [9], the use of spherical Hankel functions to compute the free-space solution for $\mathrm{Im}(A_\phi)$, i.e., the imaginary part of (1a), presents no particular difficulty in either the near or far field zones. The spherical solutions for $\mathrm{Im}(A_\phi)$ and associated derived quantities such as $\mathrm{Re}(E_\phi)$ converge over a very wide range of parameters. On the other hand, difficulties may arise in the use of spherical Hankel functions for computing $\mathrm{Re}(A_\phi)$ and associated parameters such as $\mathrm{Im}(E_\phi)$, $\mathrm{Re}(B_\rho)$ and $\mathrm{Re}(B_z)$ in the near field. This section compares the performance of the proposed series in the near field with known solutions based on spherical Hankel functions. All special functions and numerical integrations used in the following sections are computed in double precision using standard Matlab routines [38].

Figure 2(a) shows contours of constant $\mathrm{Im}(E_\phi)$ computed on a 101×101 spatial grid for a free-space region in the ρ-z plane, using the imaginary part of the series (23) involving elliptic integrals. The loop parameters are $a = 1$ m, $I = 1$ A and a frequency of 30 MHz. Figure 2(a) spans regions having both $r < a$ and $r > a$. $\mathrm{Im}(E_\phi)$ was computed to satisfy at least one of the following targeted tolerances; (i) a relative tolerance of 10^{-7}, or (ii) an absolute tolerance of 10^{-10} V/m. Agreement with the calculation via direct numerical integration of Equation (1a), performed using Matlab "integral" function [39] with the same tolerances, was obtained for all computed points over the entire zone in Figure 2(a).

A computation of $\mathrm{Im}(E_\phi)$ over the zone in Figure 2(a) was also performed using spherical Hankel functions ([6], Equation (61)), with the same targeted tolerances. The spherical series agrees with both the elliptic series and the direct integration, except in the shaded grey region in Figure 2(a) near the loop where the spherical solution exceeds a relative error of 10^{-5}. Failure to achieve the desired tolerance in the shaded zone is due to machine overflow associated with computation of high order spherical terms. The onset of this overflow is abrupt; virtually the entire shaded zone corresponds to the failure to achieve any meaningful accuracy. For this particular case, the boundary of the shaded zone is found to very closely correspond to the toroidal surface defined by $x^2 = 0.965$, indicated by the dotted contour plotted at the edge of the shaded zone. Figure 2(b) shows the same spatial zone and loop parameters as Figure 2(a), except with a frequency of 300 MHz. The spherical solutions similarly fail near the loop contour, but inside a smaller toroidal surface defined by $x^2 = 0.978$.

Figure 3 shows a similar analysis to that in Figure 2, except that the calculation is performed over a larger region in the ρ-z plane. In this case the elliptic series agrees with direct integration, except for the grey shaded areas most distant from the loop where the series solution exceeds an error of 10^{-5}, despite a targeted relative tolerance of 10^{-7}. In this case the loss of precision is gradual rather than abrupt and is associated with the computation of an increasing number of terms in the elliptic series. When the product $k_0 R_o$ is large the magnitude of initial terms in the alternating series increase to a maximum, before dropping as the factorial denominators act to reduce the magnitude of the later terms. For such cases the loss of accuracy of the accumulated sum is due to the limited numerical precision of the larger terms in the sum, rather than a basic convergence problem of the series. This is similar to the behaviour for the nested Legendre series described in [9]. For the calculations and tolerances used here, the onset of reduced

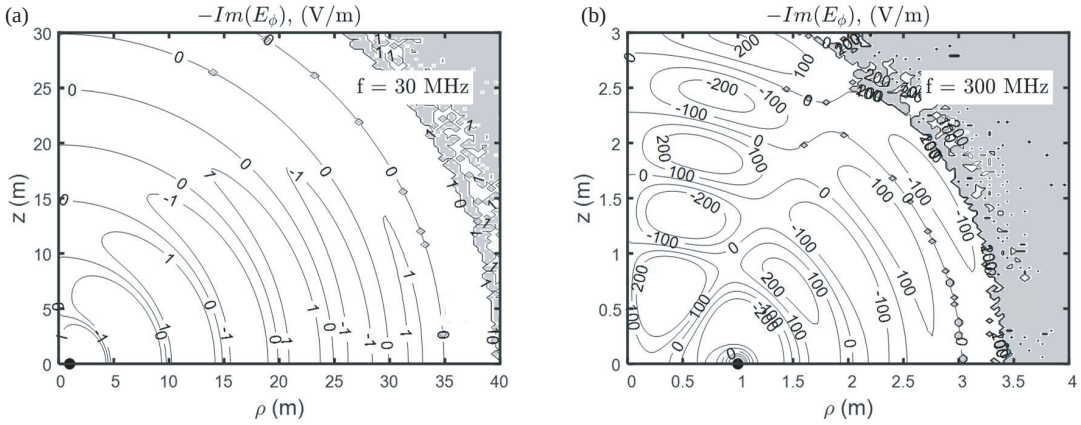

FIGURE 3. Contour plot of $-\mathrm{Im}(E_\phi)$ for a loop with $a = 1$ m and $I = 1$ A using Equations (17d) and (23) over extended spatial zones. (a) 30 MHz and (b) 300 MHz. Shaded zones indicate loss of accuracy for computations using the proposed series solutions.

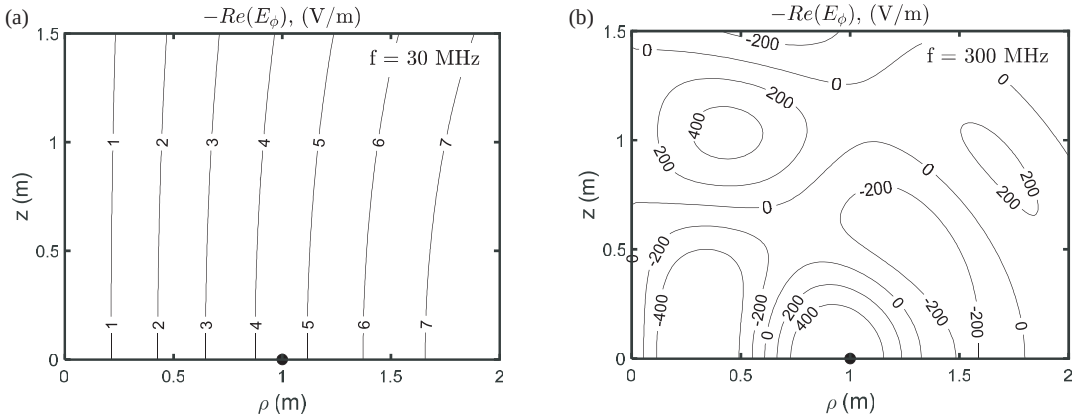

FIGURE 4. Contour plot of $-\mathrm{Re}(E_\phi)$ for a loop with $a = 1$ m and $I = 1$ A in the same extreme near-field zone of Figure 2, using Equations (21) and (23). (a) 30 MHz and (b) 300 MHz.

accuracy occurs for regions greater than approximately several wavelengths from the loop.

All electric and magnetic field expressions in this paper for a given field point can be completed with one single computation of $K(x)$ and $E(x)$, followed by application of the associated recursions and finite sums. The computation of each recursion or sum can be achieved without recourse to direct evaluation of factorials or high order power terms, by updating successive factorials or powers based on previous values as the series progresses. Using this basic numerical approach, the computations using the elliptic series over the spatial zone and parameters in Figure 2 are faster than direct integration by over a factor of 100.

In addition, for spatial regions in Figure 2 where computation of the elliptic and spherical series both achieve the targeted tolerances, the elliptic series is found to be faster than the spherical series by approximately a factor of 20. Similarly, for the common zones of acceptable tolerance Figure 3, the elliptic series is faster by approximately a factor of 5–10. The relative speed of the computations performed using the two series can depend on details of the coding, but the difference observed between elliptic and spherical series appears to be related to the requirement for new half-integer Hankel function calls for each ascending term in the spherical series. This could possibly be avoided by casting the spherical series as a stable recursion.

It is also worth noting that computation of the real part of E_ϕ in the extreme near field, using the finite sum (21) and series (23), is faster than the spherical Hankel computation. Figure 4 shows the computation of $\mathrm{Re}(E_\phi)$ using the finite sum, to a relative tolerance of 10^{-7}, over the same spatial zone and parameters as for Figure 2. Agreement between the finite sum, direct integration and spherical series to the same tolerance is obtained across the entire zone and parameter ranges, however, the finite sum is approximately 20 times faster than the spherical series and much faster than direct integration.

The computation of B_ρ and B_z exhibits similar behaviour as observed for E_ϕ, where the elliptic series and finite sums provide efficient computation in the near field but gradual decline in performance in the far field. Figures 5(a) and (b) show the computation of $\mathrm{Re}(B_\rho)$ and $\mathrm{Re}(B_z)$ using the elliptic recursions (30) and (36) respectively, for the same spatial zone and parameters as for Figure 2(b). Agreement with direct integration to relative tolerance of 10^{-7} is obtained for the entire zone in Figure 5, where the direct integrals used for the comparison are generated through application of derivatives (28) and (29) to (1a).

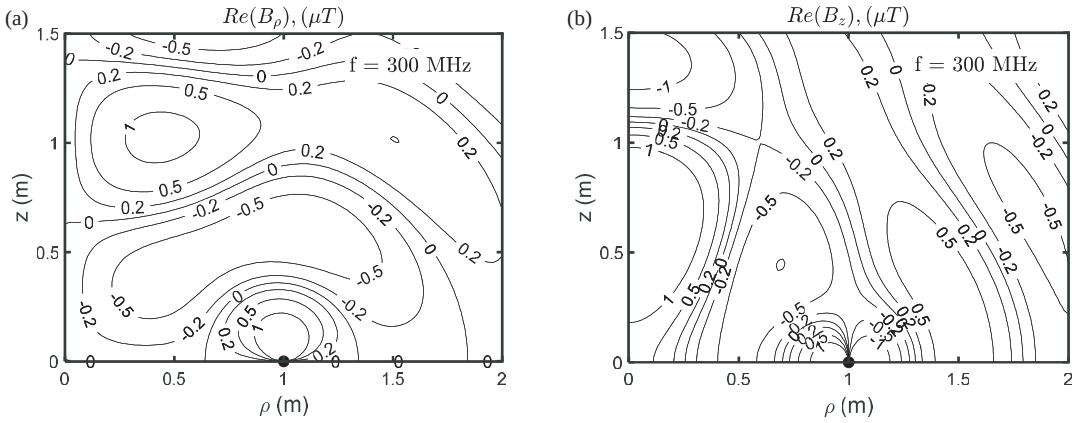

FIGURE 5. Contour plot of real part of magnetic fields for a loop with $a = 1\,\text{m}$, $I = 1\,\text{A}$ and frequency 300 MHz in the same extreme near-field zone of Figure 2(b). (a) $\text{Re}(B_\rho)$ using Equation (30). (b) $\text{Re}(B_z)$ using Equation (36).

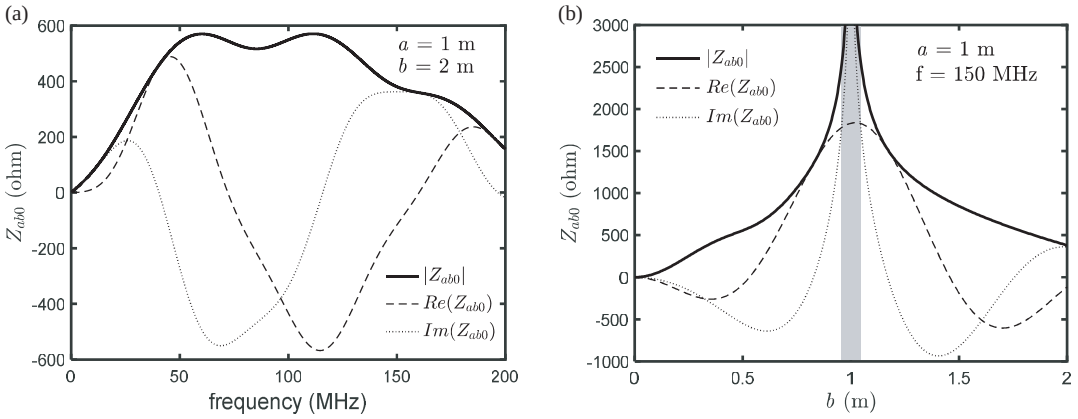

FIGURE 6. Mutual impedance for loops on a half space calculated using Equation (71). (a) Mutual impedance between two loops with $a = 1\,\text{m}$ and $b = 2\,\text{m}$ versus frequency. (b) Mutual impedance between two loops at frequency 150 MHz, with $a = 1\,\text{m}$ and varying b. Half space parameters are $\epsilon_1 = 5\epsilon_o$ and $\sigma_1 = 0.002\,\text{Sm}^{-1}$.

6. RESULTS FOR LOOPS ON A HALF SPACE

The mutual coupling of loops lying on an earth half space is of interest in designing compact coaxial arrays for efficiently exciting zero field magnetic resonances to characterise localised mineralised zones. In hard rock mining, magnetic resonance measurement applications are generally characterised by porphyry granite host rock, involving the use of moderate sized arrays up to several metre radius and operation frequencies of tens of megahertz. Figure 6(a) shows the mutual impedance Z_{ab0} between two loops lying on a half space as a function of frequency, with $a = 1\,\text{m}$ and $b = 2\,\text{m}$, computed to a relative tolerance of 10^{-5} using the power series in Equation (71). The half space is characterised by $\epsilon_1 = 5\epsilon_o$ and $\sigma_1 = 0.002\,\text{Sm}^{-1}$, consistent with indicative values for dielectric constant and loss tangents reported for relatively dry granite [40] at VHF band. The results agree with an alternative expression based on spherical Hankel functions provided in [28], Equation (16).

Figure 6(b) shows Z_{ab0} computed using (71), for a fixed frequency of 150 MHz, where $a = 1\,\text{m}$ and b is varied from zero to 2 m. Generally, a pattern of complementary performance is observed for the power series and Hankel series, similar to the free space case described in the previous section. The Hankel and power series agrees for all cases to within a targeted relative tolerance of 10^{-5}, except in the small grey shaded zone very close to the loop where the Hankel series exhibits rapid onset of overflow. On the other hand, for the parameters used in Figure 6(b), the power series gradually looses accuracy for $b > 2\,\text{m}$. The power series provides efficient computations for positions closer to the loop while the Hankel series has rapidly improving efficiency in the intermediate and far field.

Figures 7(a) and (b) respectively show the real and imaginary parts of the quantity $Z_{aa0} - j\mu_0\omega a T_\delta$ (solid lines), for a loop with $a = 1\,\text{m}$, sitting on a half space having the same parameters as in Figure 6. This quantity is the total loop self-impedance given by (76), less the quasistatic (non-radiative) thin wire approximation for the otherwise divergent component of the loop reactance due to the idealised infinitesimal loop wire radius. In a practical measurement of the self-impedance of a thin loop on a half space, the quasistatic term can be easily accounted for through calculation or measurement at low frequency.

Also plotted in Figure 7 (dashed lines) are the real and imaginary parts of $Z_{aa} - j\mu_0\omega a T_\delta$, the self-impedance of the same loop isolated in free space as given by (25), less the thin wire reactance approximation. The difference between the respec-

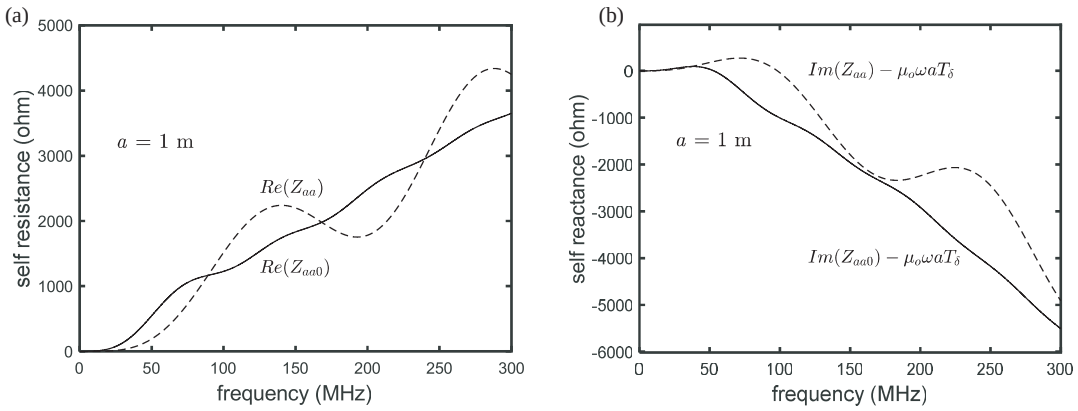

FIGURE 7. Self-impedance Z_{aa0} of a loop with $a = 1$ m on a half space (solid line) and self-impedance Z_{aa} in free space (dashed line) as a function of frequency. (a) Self resistance and (b) self reactance, less the quasistatic component. Half space parameters are $\epsilon_1 = 5\epsilon_o$ and $\sigma_1 = 0.002\,\mathrm{Sm}^{-1}$.

tive curves in Figure 7 is $Z_{aa0} - Z_{aa}$, which represents the effects imparted only by the presence of the half space interface. This impedance difference is given by $-j\omega\mu_o\pi a^2 Q$, where Q is the integral (60) with $\rho = a$, $h = 0$ and $z \to 0$. As a check of accuracy of the series, the differences in respective curves in Figure 7 were compared with the numerical integration of (60), with $z = 10^{-8}$ m to allow numerical convergence. Agreement with the numerical integration, targeted to a relative tolerance of 10^{-5}, was obtained for all values of $Z_{aa0} - Z_{aa}$ in Figures 7(a) and (b).

Figure 8 shows the real and imaginary parts of the axial magnetic field $B_{T0z}(\rho)$ at the interface, generated by a loop with $a = 1\,\mathrm{m}$ and $I = 1\,\mathrm{A}$, calculated using the power series (78) with the same parameters as in Figure 6(b). The result agrees with numerical integration of (77) to within a targeted relative tolerance of 10^{-5}. The numerical integration was performed using Matlab Gauss-Konrod quadrature with $h = 0$ and $z = 10^{-8}\,\mathrm{m}$. The field was also calculated using a series based on spherical Hankel functions in [27], Equation (51). Agreement with the power series was obtained, except for the radial region indicated by grey shading in Figure 8, where the

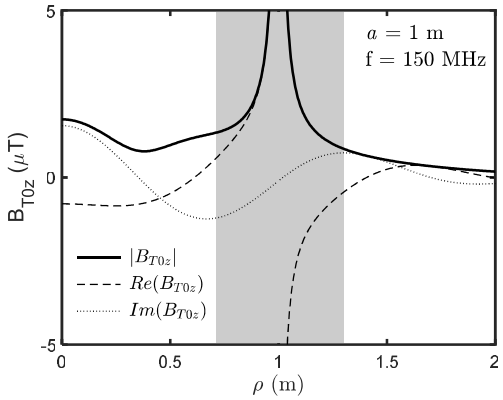

FIGURE 8. Axial field B_{T0z} on a half space interface generated by of a loop with $a = 1\,\mathrm{m}$, $I = 1\,\mathrm{A}$ and frequency 150 MHz sitting on the half space. Real part (dashed line), imaginary part (dotted line) and magnitude (solid line). Half space parameters are $\epsilon_1 = 5\epsilon_o$ and $\sigma_1 = 0.002\,\mathrm{Sm}^{-1}$.

calculation using spherical functions exceeds the targeted tolerance, mainly due to overflow, in similar fashion to that observed for free space field calculations. Likewise, for the parameters adopted in Figure 8 the power series accuracy gradually declines at radii beyond 2 m. For the range in Figure 8 where both the power series and spherical Hankel series agree, the power series appears to have a speed advantage, exceeding approximately one order of magnitude for the radial range 0.45–1.8 m for the specific parameters adopted in Figure 8. It should be noted however that such a comparison depends on coding details and the potential use of accelerating methods for either series.

7. CONCLUSION

Exact expressions for the electric and magnetic field generated by a thin, time varying uniform loop current in free space have been derived. The expressions take the form of a power series in wavenumber with coefficients involving elliptic integrals or finite sums. The series have been numerically compared to equivalent integral expressions and alternative series based on spherical Hankel functions. The comparison demonstrates the efficient field computation for spatial zones both within the loop radius and generally extending several free-space wavelengths from the loop contour. The expressions have been adapted to provide expressions for the electric and axial magnetic field at a half space interface, which have been verified for specific half-space parameters against integral expressions and spherical Hankel series. The derived series also allow for relatively simple expressions for the mutual impedance between coaxial loops lying on a half space and the radiative component of the self impedance of a single loop on a half space.

REFERENCES

[1] King, R. W. P., "The loop antenna for transmission and reception," *Antenna Theory*, R. E. Collins and F. J. Zucker, Eds, Part I, Chapter 11, McGraw-Hill, New York, 1969.

[2] Balanis, C. A., *Antenna Theory: Analysis and Design*, 3rd ed., John Wiley & Sons, Hoboken, New Jersey, 2005.

[3] Smith, G. S., "Loop antennas," *Antenna Engineering Handbook*, 4th ed., Chapter 5, McGraw-Hill, New York, 2007.
[4] Foster, D., "Loop antennas with uniform current," *Proceedings of the IRE*, Vol. 32, No. 10, 603–607, Oct. 1944.
[5] Chang, H.-T., "Near field of a loaded circular toroidal antenna," *Applied Physics*, Vol. 3, No. 2, 149–154, 1974.
[6] Werner, D. H., "An exact integration procedure for vector potentials of thin circular loop antennas," *IEEE Transactions on Antennas and Propagation*, Vol. 44, No. 2, 157–165, Feb. 1996.
[7] Li, L.-W., M.-S. Leong, P.-S. Kooi, and T.-S. Yeo, "Exact solutions of electromagnetic fields in both near and far zones radiated by thin circular-loop antennas: A general representation," *IEEE Transactions on Antennas and Propagation*, Vol. 45, No. 12, 1741–1748, 1997.
[8] Overfelt, P. L., "Near fields of the constant current thin circular loop antenna of arbitrary radius," *IEEE Transactions on Antennas and Propagation*, Vol. 44, No. 2, 166–171, 1996.
[9] Conway, J. T., "New exact solution procedure for the near fields of the general thin circular loop antenna," *IEEE Transactions on Antennas and Propagation*, Vol. 53, No. 1, 509–517, Jan. 2005.
[10] Maxwell, J. C., *A Treatise on Electricity and Magnetism*, 3rd ed., Vol. 2, Sec. 701, 338–340, Oxford University Press, London, 1892.
[11] Rosa, E. B. and F. W. Grover, "Formulas and tables for the calculation of mutual and self inductance (revised)," *Bulletin of the Bureau of Standards*, Vol. 8, No. 8, 111, 1912.
[12] Carter, G. W., S. C. Loh, and C. Y. K. Po, "The magnetic fields of systems of currents circulating in a conducting ring," *The Quarterly Journal of Mechanics and Applied Mathematics*, Vol. 18, No. 1, 87–106, 1965.
[13] Ivaska, V., V. Jonkus, and V. Palenskis, "Magnetic field distribution around a superconducting torus," *Physica C*, Vol. 319, No. 1-2, 79–86, Jun. 1999.
[14] Pocklington, H. C., "Electrical oscillations in wires," *Proceedings of the Cambridge Philosophical Society*, Vol. 9, 324–332, 1897.
[15] Storer, J. E., "Impedance of thin-wire loop antennas," *Transactions of the American Institute of Electrical Engineers, Part I: Communication and Electronics*, Vol. 75, No. 5, 606–619, 1956.
[16] Wu, T. T., "Theory of the thin circular loop antenna," *Journal of Mathematical Physics*, Vol. 3, No. 6, 1301–1304, 1962.
[17] Greene, F. M., "The near-zone magnetic field of a small circular-loop antenna," *Journal of Research of the National Bureau of Standards*, Vol. 71C, No. 4, 319–326, 1967.
[18] Iizuka, K., R. King, and C. Harrison, "Self- and mutual admittances of two identical circular loop antennas in a conducting medium and in air," *IEEE Transactions on Antennas and Propagation*, Vol. 14, No. 4, 440–450, Jul. 1966.
[19] Ito, S., N. Inagaki, and T. Sekiguchi, "An investigation of the array of circular-loop antennas," *IEEE Transactions on Antennas and Propagation*, Vol. 19, No. 4, 469–476, 1971.
[20] Wait, J. R., "Insulated loop antenna immersed in a conducting medium," *Journal of Research of the National Bureau of Standards*, Vol. 59, No. 2, 133–137, 1957.
[21] Kraichman, M. B., "Impedance of a circular loop in an infinite conducting medium," *Journal of Research of the National Bureau of Standards — D. Radio Propagation*, Vol. 66D, No. 4, 499–503, 1962.
[22] Wait, J. R., "Mutual electromagnetic coupling of loops over a homogeneous ground — An additional note," *Geophysics*, Vol. 21, No. 2, 261–500, Apr. 1956.
[23] Wait, J. R., "The electromagnetic fields of a horizontal dipole in the presence of a conducting half-space," *Canadian Journal of Physics*, Vol. 39, No. 7, 1017–1028, 1961.
[24] Galejs, J., "Input resistance of horizontal loops above a conducting ground plane," *Radio Science*, Vol. 6, No. 11, 1011–1013, 1971.
[25] Wait, J. R. and K. P. Spies, "Low-frequency impedance of a circular loop over a conducting ground," *Electronics Letters*, Vol. 15, No. 9, 346–348, 1973.
[26] Parise, M., "Quasi-static vertical magnetic field of a large horizontal circular loop located at the earth's surface," *Progress In Electromagnetics Research Letters*, Vol. 62, 29–34, 2016.
[27] Parise, M., M. Muzi, and G. Antonini, "Loop antennas with uniform current in close proximity to the earth: Canonical solution to the surface-to-surface propagation problem," *Progress In Electromagnetics Research B*, Vol. 77, 57–69, 2017.
[28] Muzi, M., "An exact expression for the mutual impedance between coaxial circular loops on a homogeneous ground," *Progress In Electromagnetics Research Letters*, Vol. 81, 65–70, 2019.
[29] Parise, M., "On the voltage response of homogeneous earth models in central loop electromagnetic sounding," *International Journal of Antennas and Propagation*, Vol. 2022, Article ID 8294000, 2022.
[30] Bruschini, C., "On the low-frequency EMI response of coincident loops over a conductive and permeable soil and corresponding background reduction schemes," *IEEE Transactions on Geoscience and Remote Sensing*, Vol. 42, No. 8, 1706–1719, 2004.
[31] Das, Y., "Effects of soil electromagnetic properties on metal detectors," *IEEE Transactions on Geoscience and Remote Sensing*, Vol. 44, No. 6, 1444–1453, 2006.
[32] Cheng, D. H. S., "The reflected impedance of a circular coil in the proximity of a semi-infinite medium," *IEEE Transactions on Instrumentation and Measurement*, Vol. 14, No. 3, 107–116, Sep. 1965.
[33] Lehmann-Horn, J. A., D. G. Miljak, L. A. O'Dell, R. Yong, and T. J. Bastow, "Rapid detection of arsenic minerals using portable broadband NQR," *Geophysical Research Letters*, Vol. 41, No. 19, 6765–6771, 2014.
[34] Coghill, P. J., A. Curtain, B. Lovric, A. McEwan, D. Milinkovic, D. G. Miljak, G. Roberts, R. Stefulj, and R. Yong, "Bulk sensing of trucks, in-pit equipment and the mine bench for preconcentration," in *Proceedings of the Preconcentration Digital Conference*, 10–11, The Australasian Institute of Mining and Metallurgy (AusIMM), 2020.
[35] Qing, X., C. K. Goh, and Z. N. Chen, "Segmented loop antenna for UHF near-field RFID applications," *Electronics Letters*, Vol. 45, No. 17, 872–873, 2009.
[36] Byrd, P. F. and M. D. Friedman, *Handbook of Elliptic Integrals for Engineers and Scientists*, Springer-Verlag, 1971.
[37] Gradshteyn, I. S. and I. M. Ryzhik, *Table of Integrals, Series, and Products*, 7th ed., Academic Press, New York, 2007.
[38] MATLAB version: 9.6.0 (R2019b), The MathWorks Inc., Natick, Massachusetts, 2019.
[39] Shampine, L. F., "Vectorized adaptive quadrature in MATLAB," *Journal of Computational and Applied Mathematics*, Vol. 211, No. 2, 131–140, 2008.
[40] Campbell, M. J. and J. Ulrichs, "Electrical properties of rocks and their significance for lunar radar observations," *Journal of Geophysical Research*, Vol. 74, No. 25, 5867–5881, 1969.